New Insights into Traffic Emissions: The Role of Hydrocarbons and Oxygenated Organic Species in Traffic-Derived Aerosol

Sanna Saarikoski[1], Minna Aurela[1], Jarkko V. Niemi[2], Luis Barreira[1], Jussi Hoivala[3], Hanna Manninen[2], Topi Rönkkö[3], Hilkka Timonen[1]

[1]Atmospheric Composition Research, Finnish Meteorological Institute, 00101 Helsinki, Finland
[2]Helsinki Region Environmental Services Authority HSY, 00066 Helsinki, Finland
[3]Aerosol Physics Laboratory, Physics Unit, Tampere University, 33014 Tampere, Finland

Supplemental material

Table S1: Average chemical composition of aerosol measured during the campaigns. Black carbon (eBC) was measured with the aethalometer (AE33, Magee Scientific, Ljubljana, Slovenia) at 880 nm. PM_1 was measured with the FIDAS (Palas GmbH, Karlsruhe, Germany) and $PM_{2.5}$ with the tapered element oscillating microbalance (TEOM 1405; Thermo Fisher Scientific, Waltham, US) in 2018. Ambient temperature and relative humidity were taken from the weather station located in Kumpula one kilometer from the street canyon site.

Measurement campaign	**PM_1** ($\mu g\ m^{-3}$)	**Chemical species** ($\mu g\ m^{-3}$)					**Meteorology**	
		OA	Sulfate	Nitrate	Ammonium	eBC	T (°C)	RH (%)
Spring 2018	7.9*	2.7	0.27	0.23	0.13	1.47	13	57
Summer-autumn 2019	3.7	2.4	0.5	0.13	0.14	1.3	17	79
Winter 2022	4.6	2.0	0.62	0.63	0.39	0.72	-1.8	90
Spring 2024	4.0	2.7	0.62	0.55	0.30	0.49	4.2	79

*$PM_{2.5}$

Table S2: Elemental ratios of the PMF factors for the campaigns.

Campaign	Factor	O:C	H:C	N:C
Spring 2018	TrOA	0.196	1.82	7.63×10^{-3}
	HOA	0.065	2.22	3.04×10^{-4}
	SV-OOA	0.511	1.72	2.89×10^{-3}
	LV-OOA	0.950	1.54	3.17×10^{-3}
Summer-autumn 2019	TrOA	0.160	1.76	1.4×10^{-2}
	HOA	0.082	2.05	1.54×10^{-4}
	SV-OOA	0.500	1.64	4.00×10^{-3}
	LV-OOA	0.710	1.60	5.20×10^{-3}
	LV-OOA-LRT	0.760	1.50	1.10×10^{-2}
	CoOA	0.250	1.86	9.20×10^{-2}
Winter 2022	TrOA	0.162	1.59	3.36×10^{-2}
	HOA	0.061	2.00	6.50×10^{-2}
	BBOA	0.165	1.84	9.72×10^{-3}
	SV-OOA	0.22	1.57	1.10×10^{-2}
	LV-OOA	0.657	1.34	4.94×10^{-2}
	LV-OOA (w/BB)	0.492	1.36	1.40×10^{-2}
Spring 2024	TrOA	0.179	1.70	1.76×10^{-2}
	HOA	0.074	2.10	7.26×10^{-3}
	SV-OOA	0.391	1.72	9.59×10^{-3}
	LV-OOA	0.743	1.51	1.9×10^{-2}
	unknown	0.752	2.51	1.77×10^{-2}

Table S3: Correlation of HOA, TrOA and SV-OOA with eBC and NOx (Pearson R) for 1-hour averaged data. eBC was measured with the AE33 and NOx with APNA 370 (Horiba).

Campaign	vs. BC			vs. NOx		
	HOA	TrOA	SV-OOA	HOA	TrOA	SV-OOA
Spring 2018	0.42	0.47	0.38	0.47	0.45	0.32
Summer-Autumn 2019	$0.64^{0.61}$	$0.40^{0.32}$	$0.30^{0.31}$	$0.65^{0.62}$	$0.37^{0.30}$	$0.095^{0.13}$
Winter 2022*	$0.48^{0.82}$	$0.53^{0.35}$	$0.49^{0.21}$	$0.59^{0.83}$	$0.57^{0.44}$	$0.36^{0.23}$
Spring 2024	0.73	0.47	0.54	0.78	0.42	0.27

*superscript values without the episode/episodes

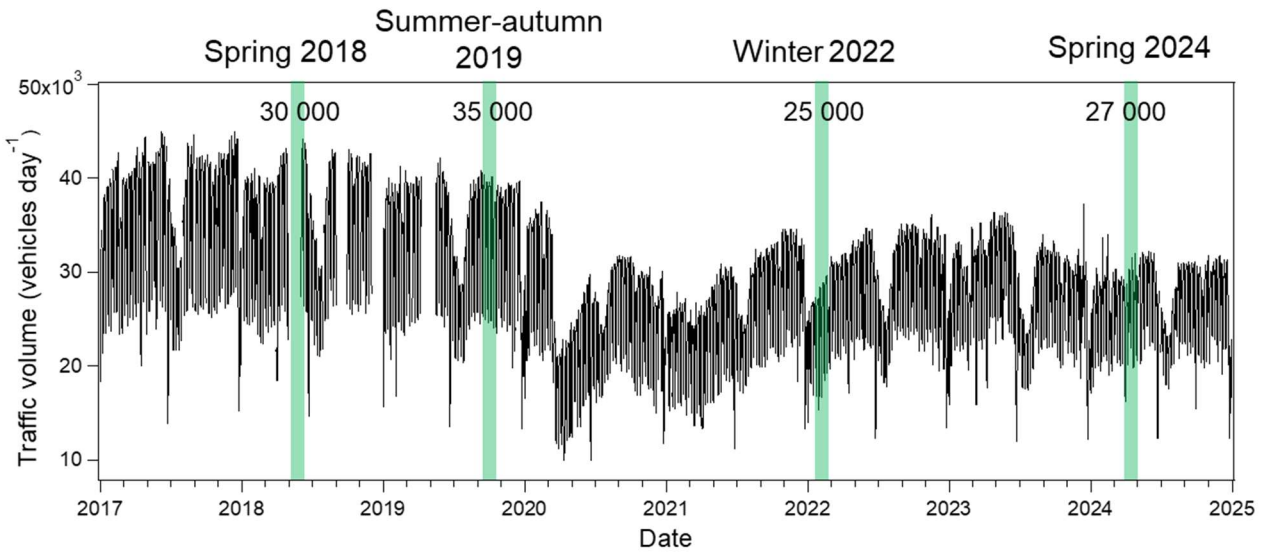

Figure S1: Traffic volumes in 2017–2024 at traffic counting site operated by the City of Helsinki. The durations of the campaigns are shown by green areas and average volumes during the campaigns by values on the top of the green areas.

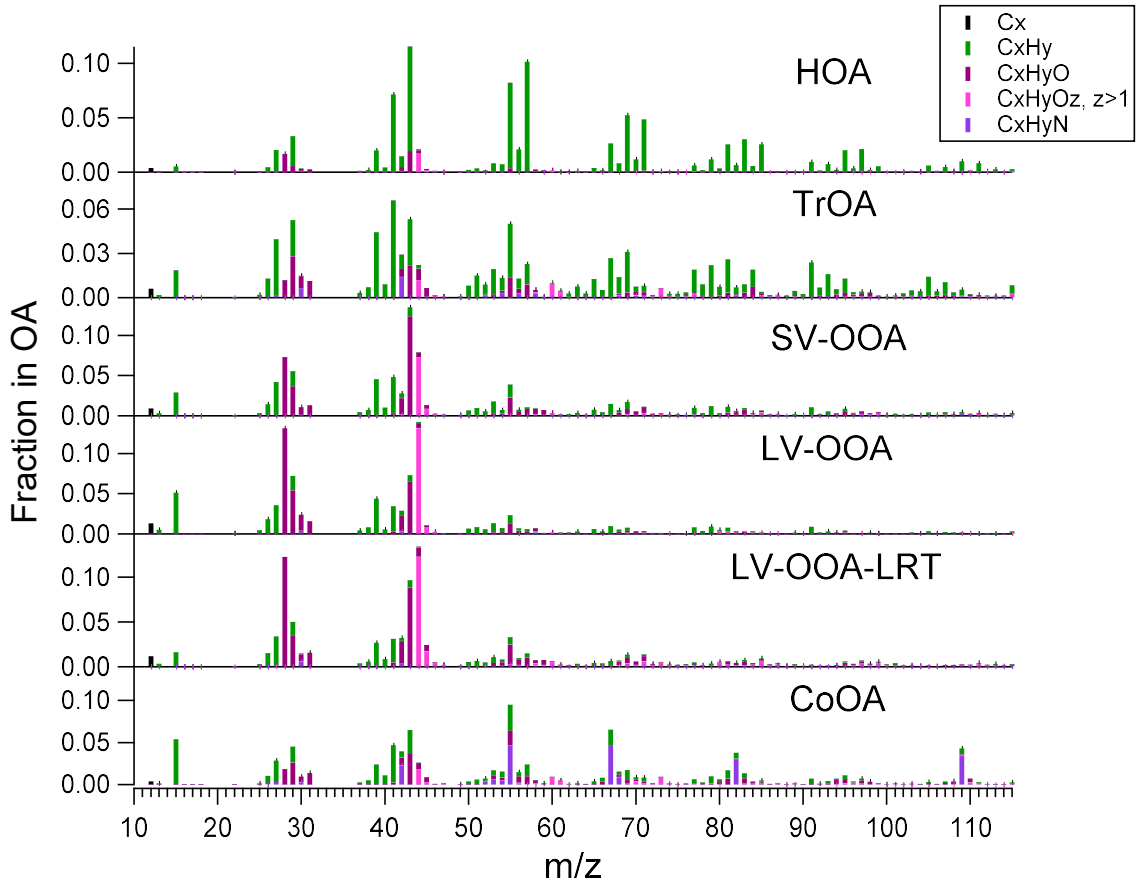

Figure S2: Mass spectra of the PMF factor for Summer-autumn 2019 data (Saarikoski et al., 2023).

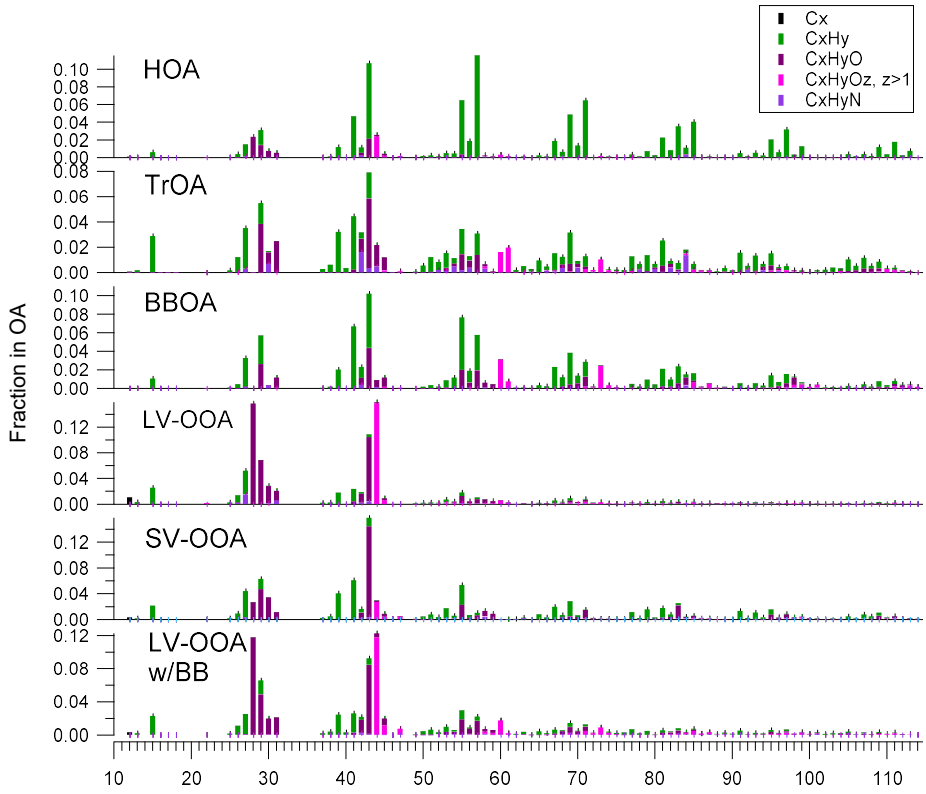

Figure S3: Mass spectra of the PMF factor for Winter 2022 data (Saarikoski et al., 2023).

Source apportionment for Spring 2018 data

The SP-AMS dataset collected in spring 2018 at the Helsinki supersite was analyzed with a positive matrix factorization (PMF) algorithm (CU AMS PMF tool v. 2.08D, Paatero and Tapper, 1994; Ulbrich et al., 2009) to identify sources and organic aerosol (OA) types. Prior to PMF analysis, the SP-AMS data were processed with ToF AMS HR Analysis 1.20O in Igor Pro 8.04. High-resolution (HR) data were averaged to 10-minute intervals, resulting in a dataset of 4440 data points.

PMF was run from 2 to 9 factors. Solutions with 6 and 7 factors were inconclusive, while the 4-factor solution provided the most reasonable results. The factors were identified as hydrocarbon-like OA (HOA), traffic-related OA (TrOA) semi-volatile oxygenated OA factor (SV-OOA), and low-volatility oxygenated OA factor (LV-OOA). Corresponding mass spectra, time series and diurnal profiles are given in Fig. S4. In the 3-factor solution, TrOA was not resolved and was split between HOA and LV-OOA. In the 5-factor solution, the additional factor presented a combination of LV-OOA and SV-OOA, and the TrOA contribution decreased from 17 to 15% compared to the 4-factor solution. Solutions with 8 and 9 factors did not yield any additional information as HOA was split into two factors.

The chemical characteristics of TrOA varied with the number of factors. The hydrogen-to-carbon ratio (H:C) remained relatively stable, whereas the oxygen-to-carbon ratio (O:C) was smallest in the 5-factor solution and largest in the 8-factor solution (Fig. S5). The relative contributions of $C_2H_4O_2^+$ (m/z 60), $C_2H_5O_2^+$ (m/z 61) and

$C_3H_5O_2^+$ (m/z 73) in TrOA also changed, the highest fractions observed in the 8-factor solution. Regarding diurnal trends, TrOA exhibited the clearest morning peak in the 4-factor solution, although its highest concentrations occurred at night across all solutions (Fig. S6a).

The 4-factor solution was further evaluated for rotational ambiguity by varying fpeak and for robustness using bootstrapping and multiple seeds. These tests confirmed that the 4-factor solution was stable.

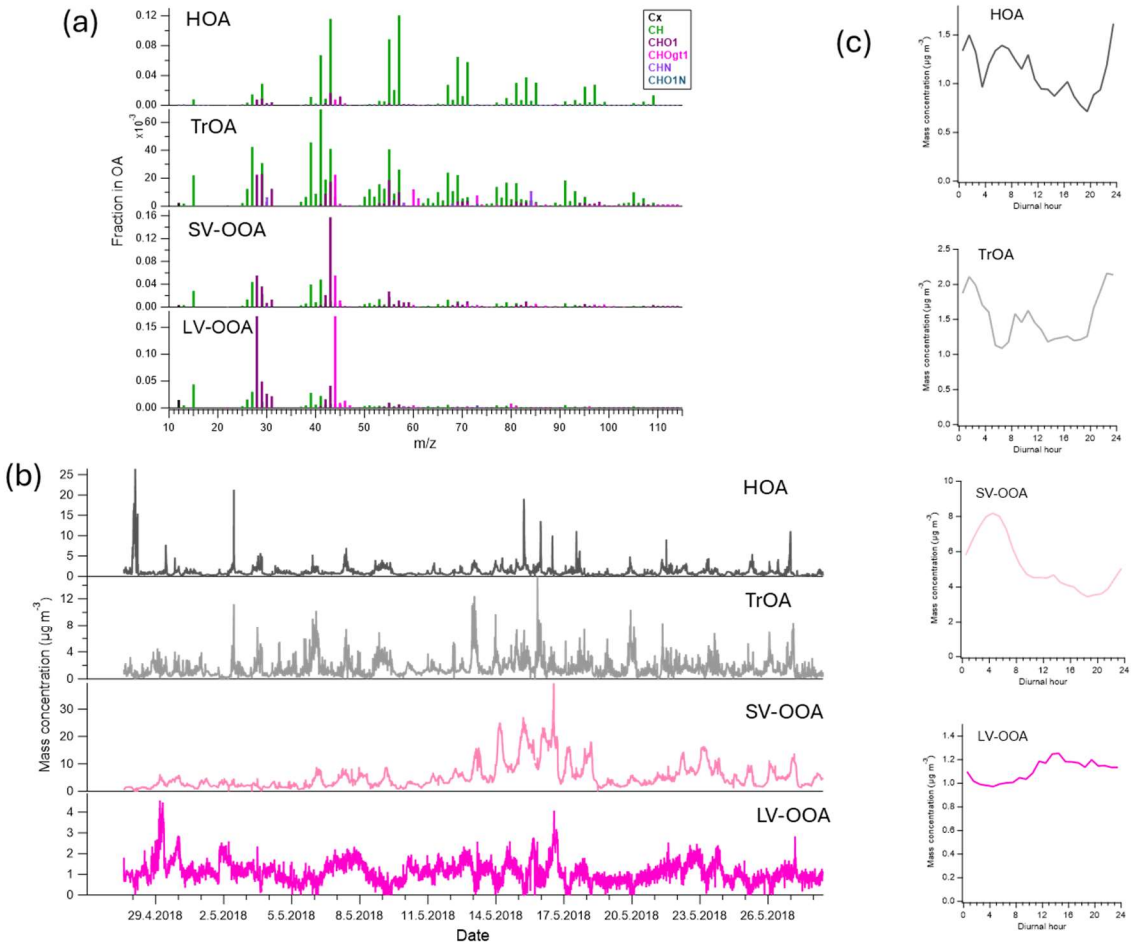

Figure S4: PMF results for the spring 2018 data. Mass spectra (a), time series (b) and diurnal trends (c).

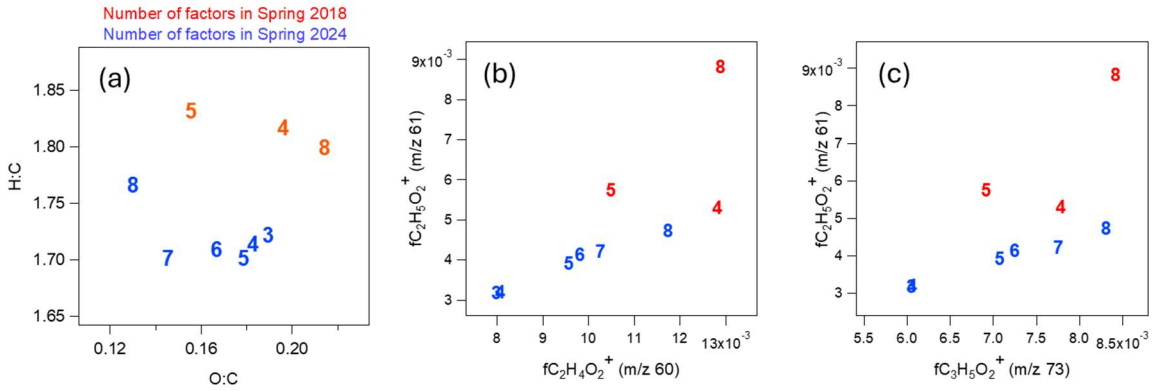

Figure S5: Elemental composition of TrOA (a), the relationship of $fC_2H_5O_2^+$ to $fC_2H_4O_2^+$ (b) and $fC_2H_5O_2^+$ to $fC_3H_4O_2^+$ (c) according to the number of PMF factors.

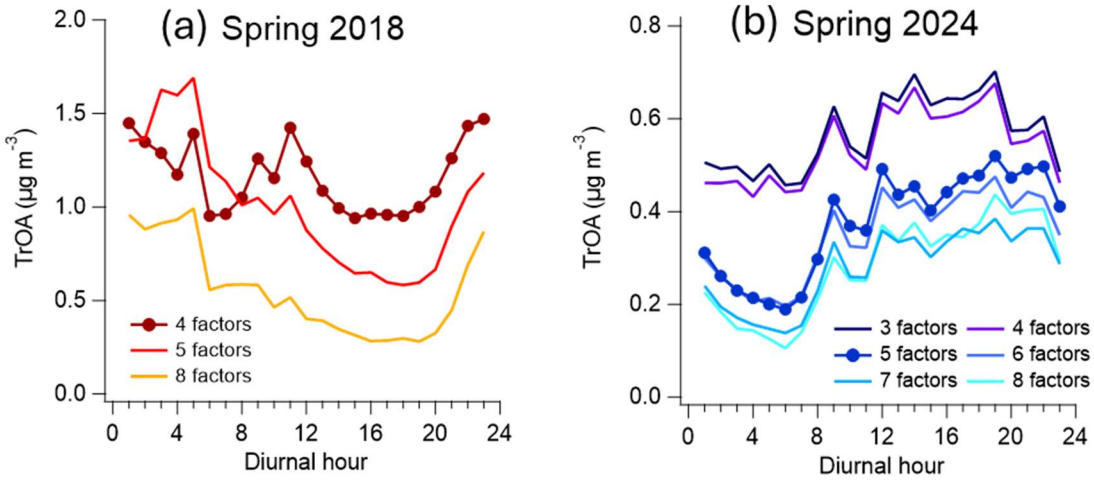

Figure S6: The diurnal trend of TrOA in Spring 2018 (a) and Spring 2024 (b) with the number of PMF factors.

Source apportionment for Spring 2024 data

The SP-AMS dataset collected in spring 2024 at the Helsinki supersite was analyzed with a positive matrix factorization (PMF) algorithm (CU AMS PMF tool v. 2.08D, Paatero and Tapper, 1994; Ulbrich et al., 2009). Before the PMF analysis, the SP-AMS data were processed with ToF AMS HR Analysis 1.26E in Igor Pro 8.04. PMF was run applied to the HR dataset at its original 1-minute time resolution, consisting of 20 100 data points. PMF was tested with 2 to 8 factors. The 5-factor solution provided the most reasonable interpretation. The factors were identified as HOA, TrOA, SV-OOA, LV-OOA, and a fifth factor of unknown origin. Mass spectra, time series and diurnal trends for these factors are shown in Fig. S7. The unknown factor appeared in three distinct 6–8 hour peaks during the nights of Fri-Sat (12-13 April), Sat-Sun (13-14 April) and Fri-Sat (26-27 April). Its mass spectrum was dominated by signals at m/z 45 ($C_2H_5O^+$) and m/z 29 (CHO^+) indicating a generally oxygenated composition. The source of this factor could not be conclusively determined, but possible explanations include

emissions from a nearby restaurant, given its occurrence on weekend nights, or road maintenance activities, as streets were being cleaned of winter sand during that period.

In the 3-factor solution, HOA and TrOA were separated, but OOA remained undivided, and the unknow factor was absent. In the 4-factor solution, the unknown factor appeared, but OOA was still grouped as one factor. In these solutions, TrOA contributions were higher (28 and 25%, respectively) compared to the 5-factor solution (18%). In the 6-factor solution, OOA split into three sub-factors, redistributing contributions from SV-OOA and LV-OOA. Further splitting occurred in the 7-factor solution, and in the 8-factor solution, the eight factor gained mass from both HOA and LV-OOA (Fig. S6b).

Compared to spring 2018 data, TrOA characteristics varied more noticeably with factor number in spring 2024 data. While H:C ratios remained rather stable across all solutions, the oxygen to carbon (O:C) ratios decreased as the number of factors increased (Fig. S5). $fC_2H_4O_2^+$ (m/z 60), $fC_2H_5O_2^+$ (m/z 61) and $fC_3H_5O_2$+ (m/z 73) in TrOA increased almost linearly with factor number (Fig. S5). Diurnal patterns of TrOA were consistent across all solutions, although its absolute concentration varied (Fig. S3).

The 4-factor solution was further investigated for rotational freedom via fpeak variation and accuracy using bootstrapping and multiple seeds. These tests showed that the 5-factor solution was robust and stable.

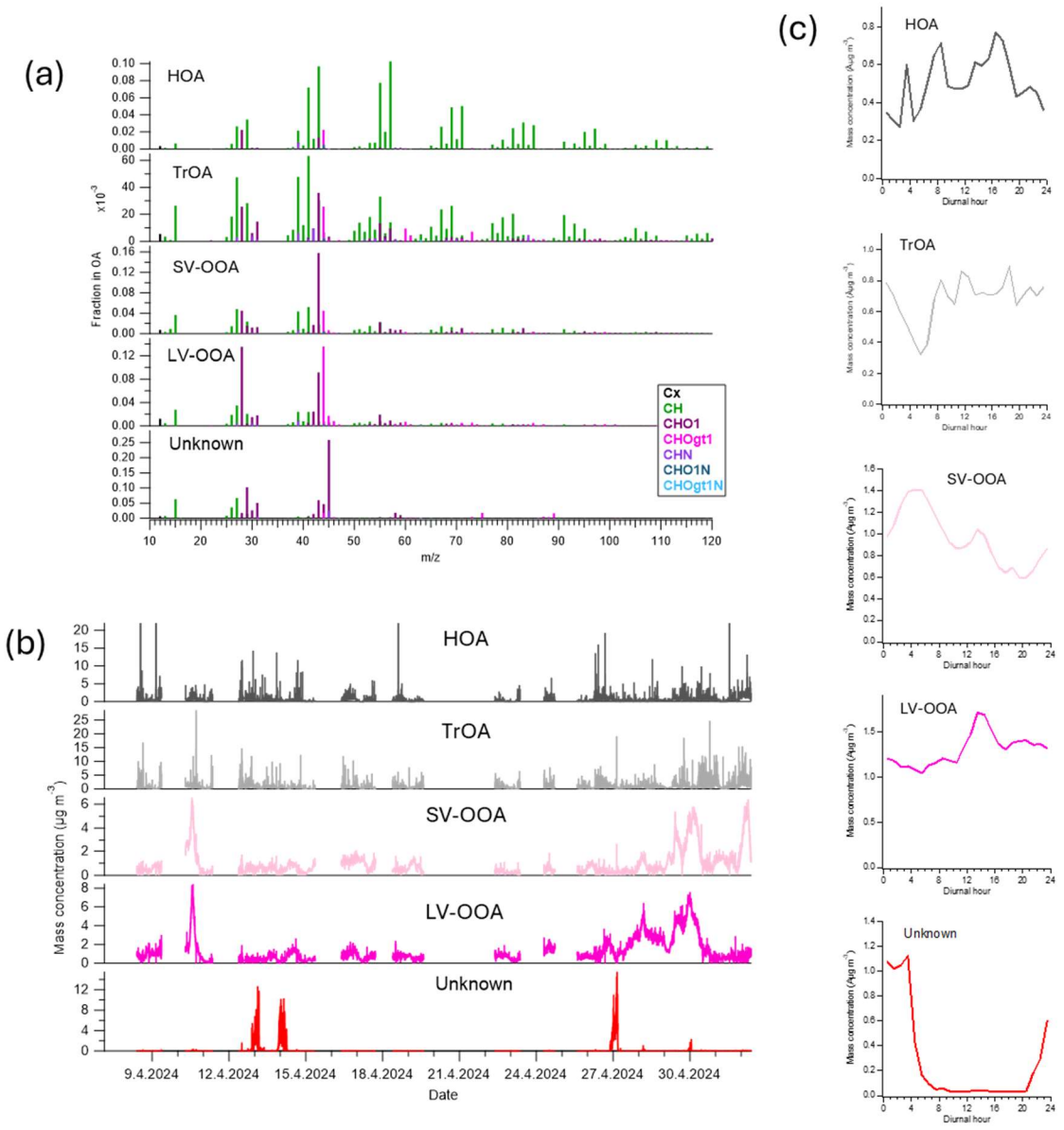

Figure S7: PMF results for the spring 2024 data. Mass spectra (a), time series (b) and diurnal trends (c).

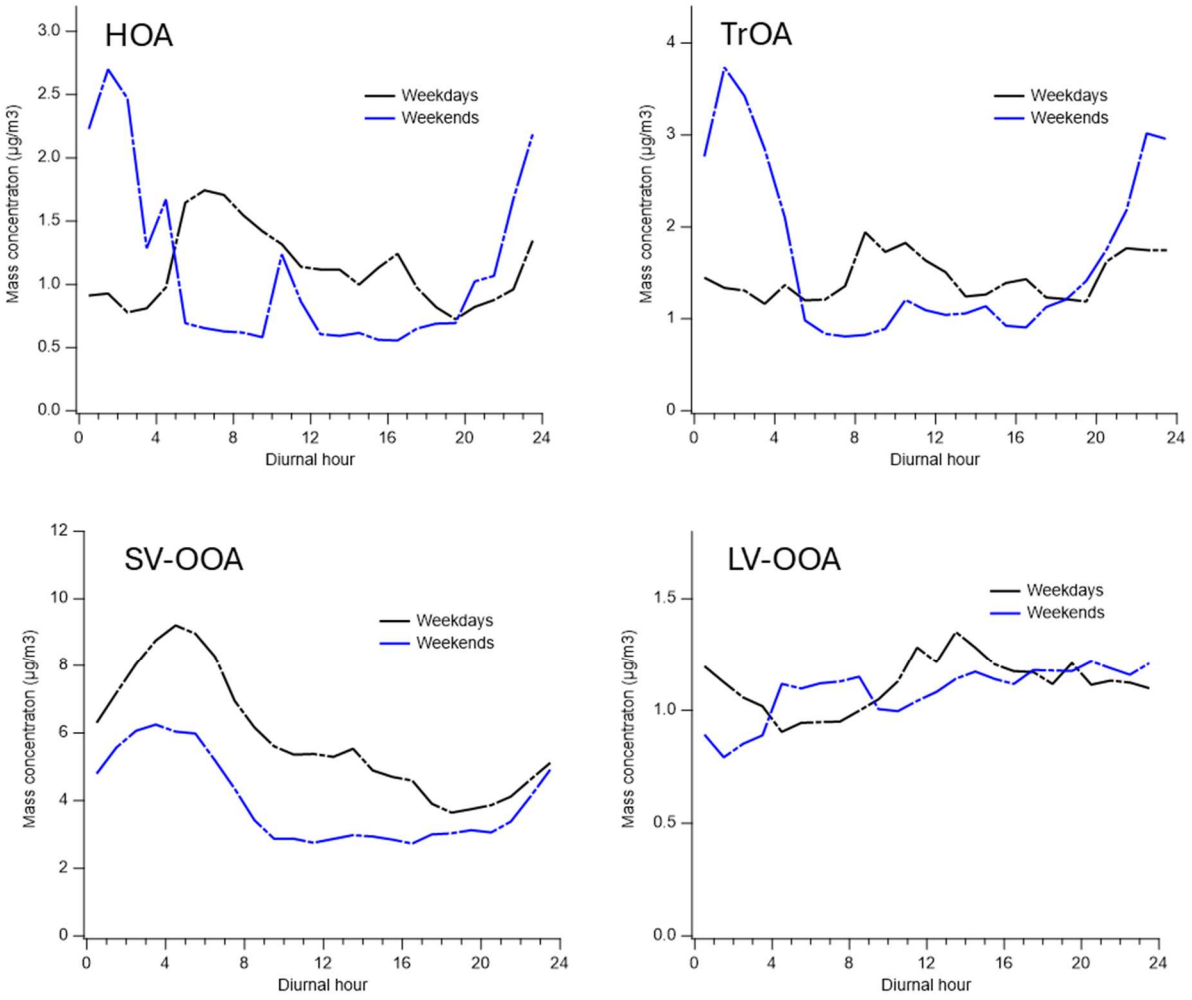

Figure S8: Average diurnal trends of the PMF factors during weekdays and weekends in Spring 2018.

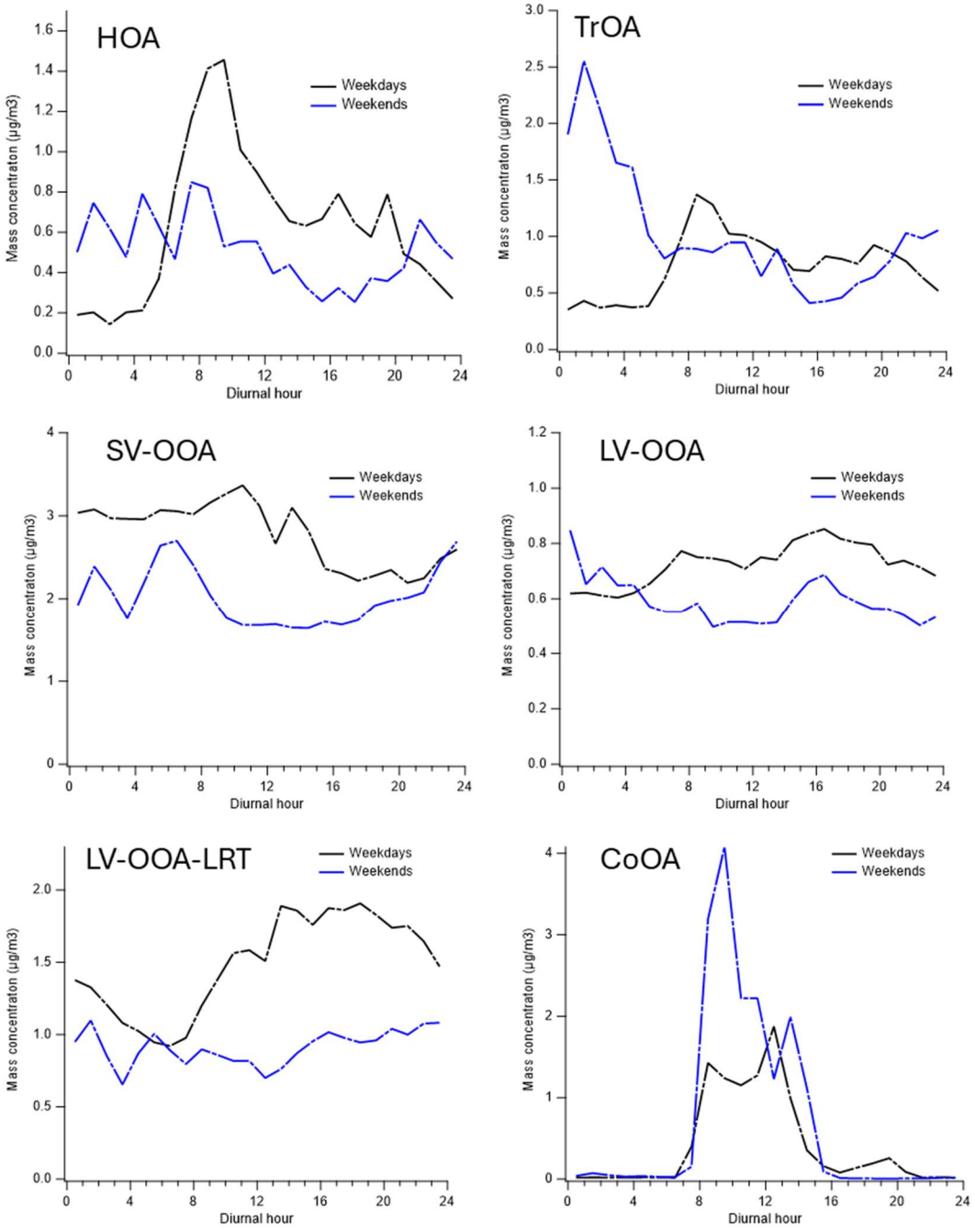

Figure S9: Average diurnal trends of the PMF factors during weekdays and weekends in Summer-autumn 2019.

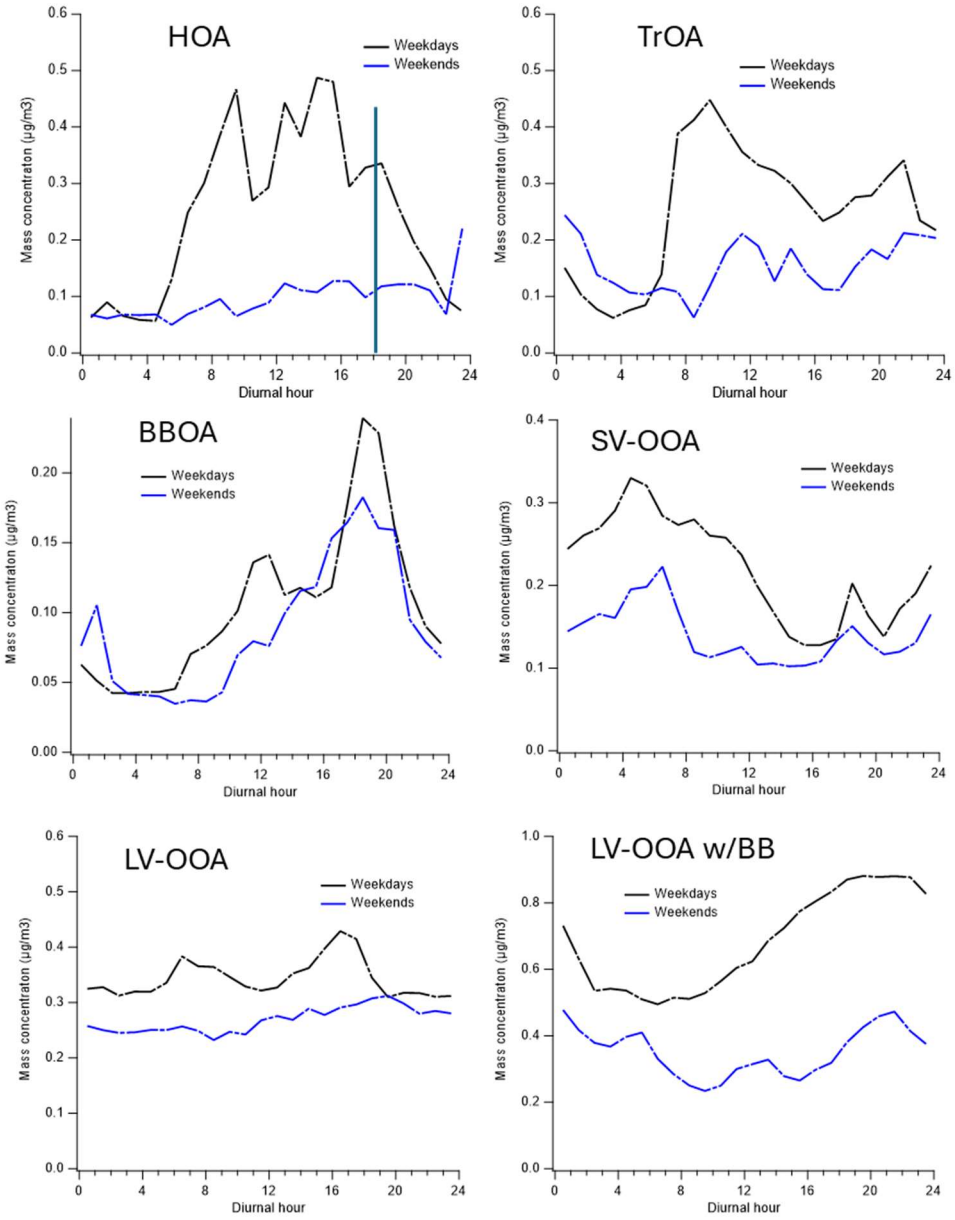

Figure S10: Average diurnal trends of the PMF factors during weekdays and weekends in Winter 2022.

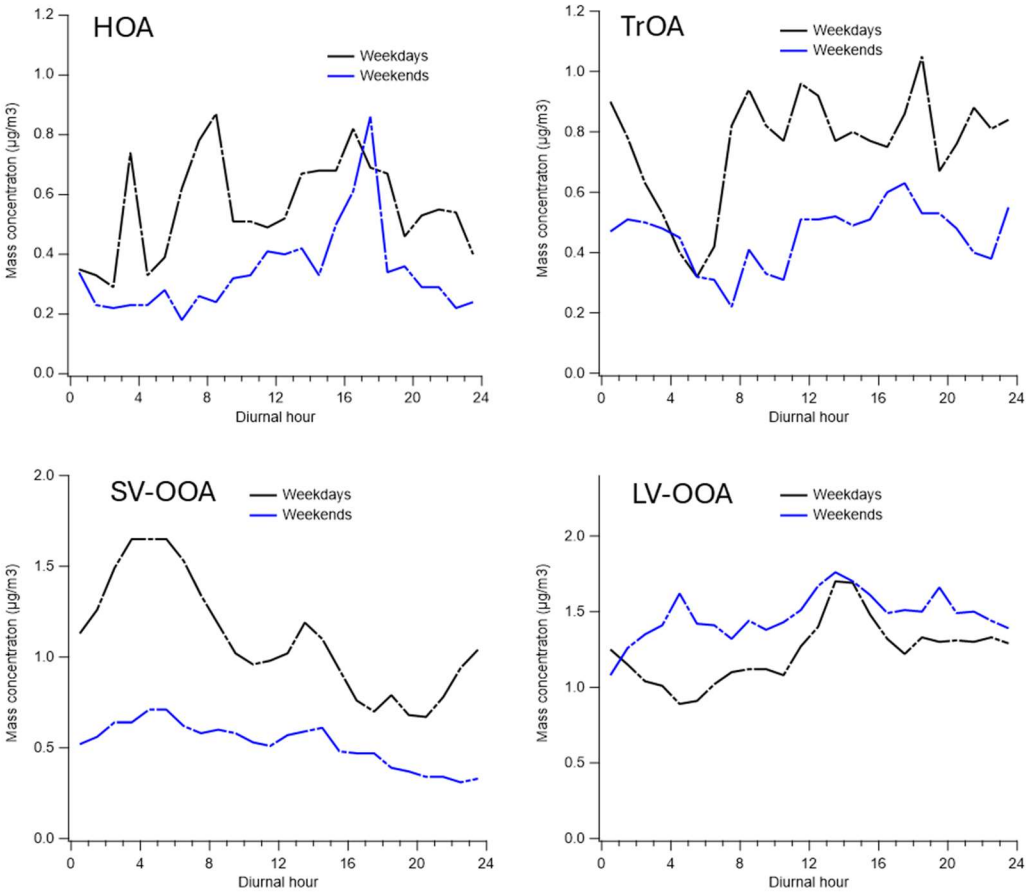

Figure S11: Average diurnal trends of the PMF factors during weekdays and weekends in Spring 2024.

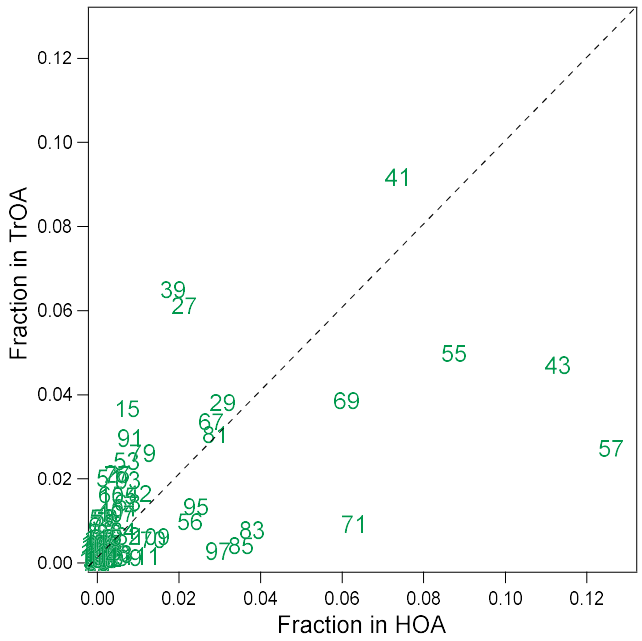

Figure S12: Comparison of the average mass spectra of TrOA and HOA in terms of hydrocarbon ions. Average mass spectra of four campaigns. Numbers indicate unit m/z values.

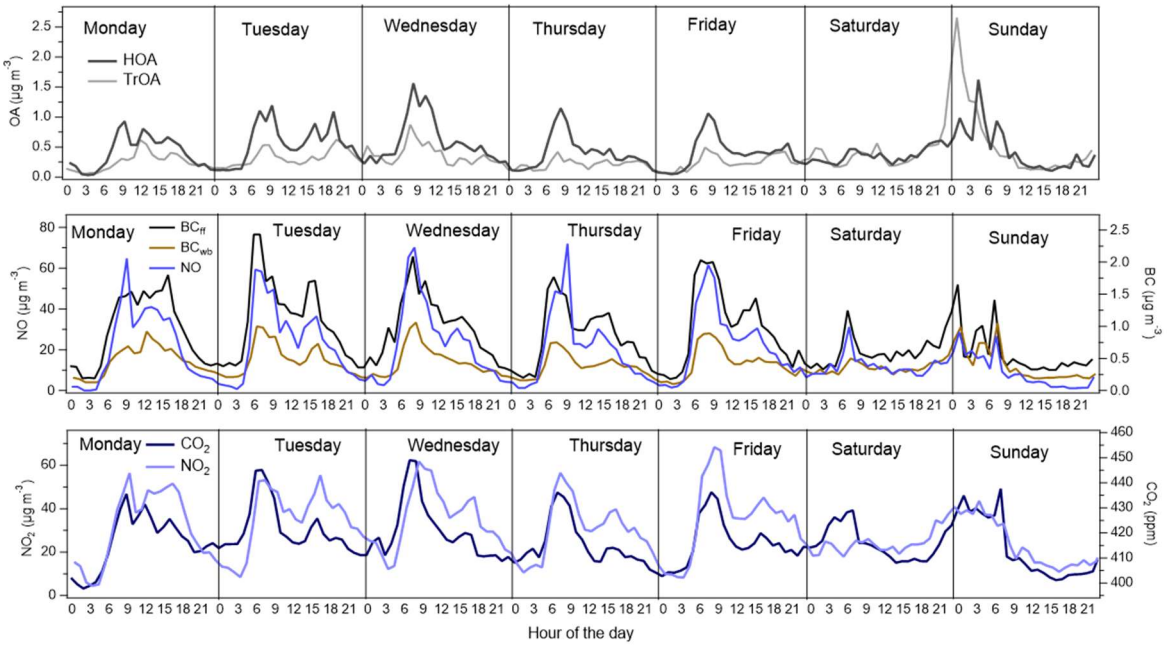

Figure S13: Average diurnal trends of HOA, TrOA, BC_{ff}, BC_{wb} NO, CO_2, and NO_2 at different days of the week during Summer-autumn 2019 campaign. Black carbon from fossil fuel combustion (BC_{ff}) and black carbon from wood burning (BC_{wb}) was measured with the aethalometer (AE33; see details in Saarikoski et al., 2024).

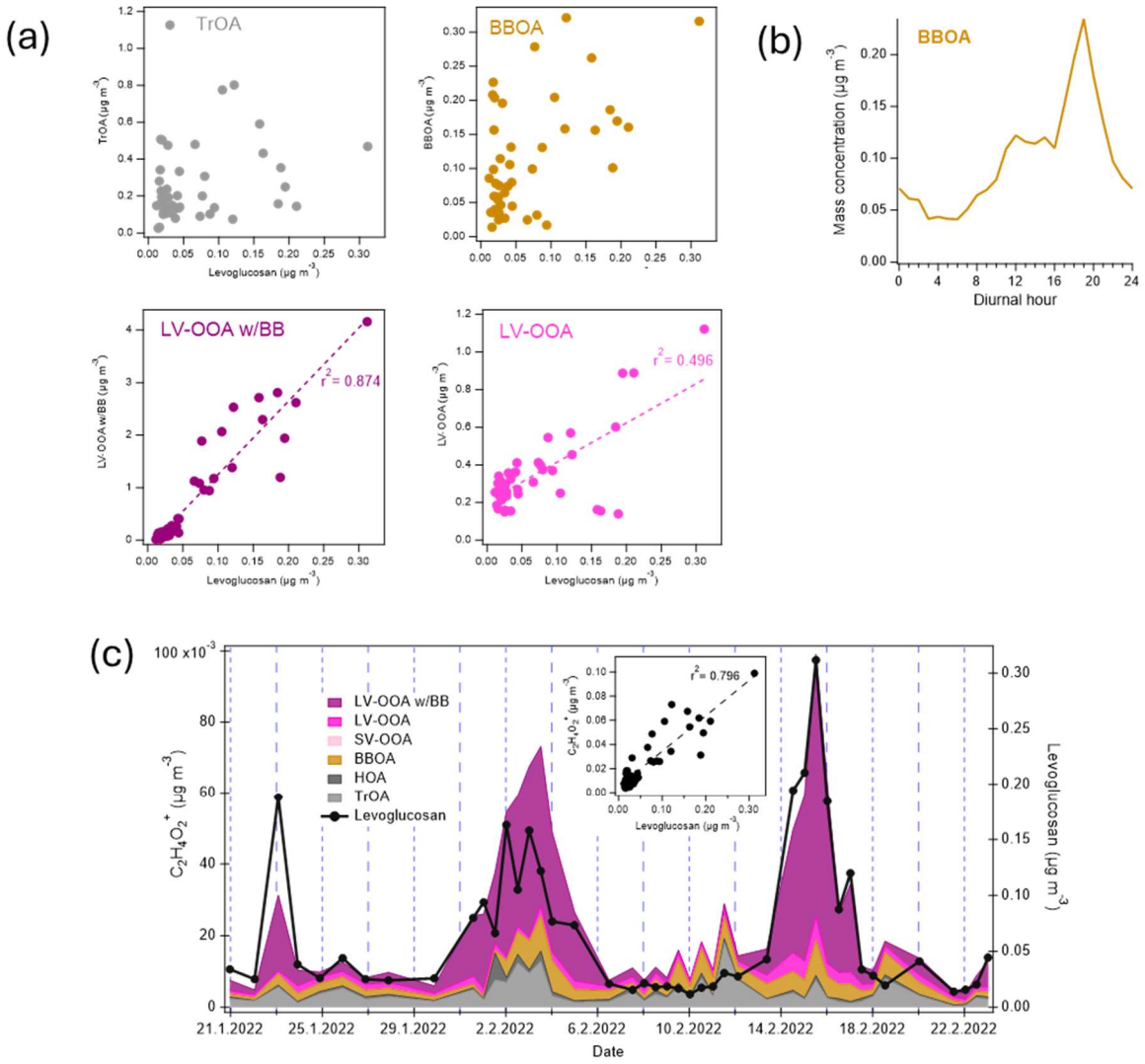

Figure S14: Correlation of selected PMF factors with the levoglucosan concentrations (a), the diurnal trend of BBOA (b), and the time series of $C_2H_4O_2^+$ divided into PMF factors (left y-axis) and the time series of levoglucosan (right y-axis, analyzed from the PM_1 filter samples) (c) during winter 2022 campaign. The details of PM_1 sampling and levoglucosan analyses have been given in Teinilä et al. (2025).

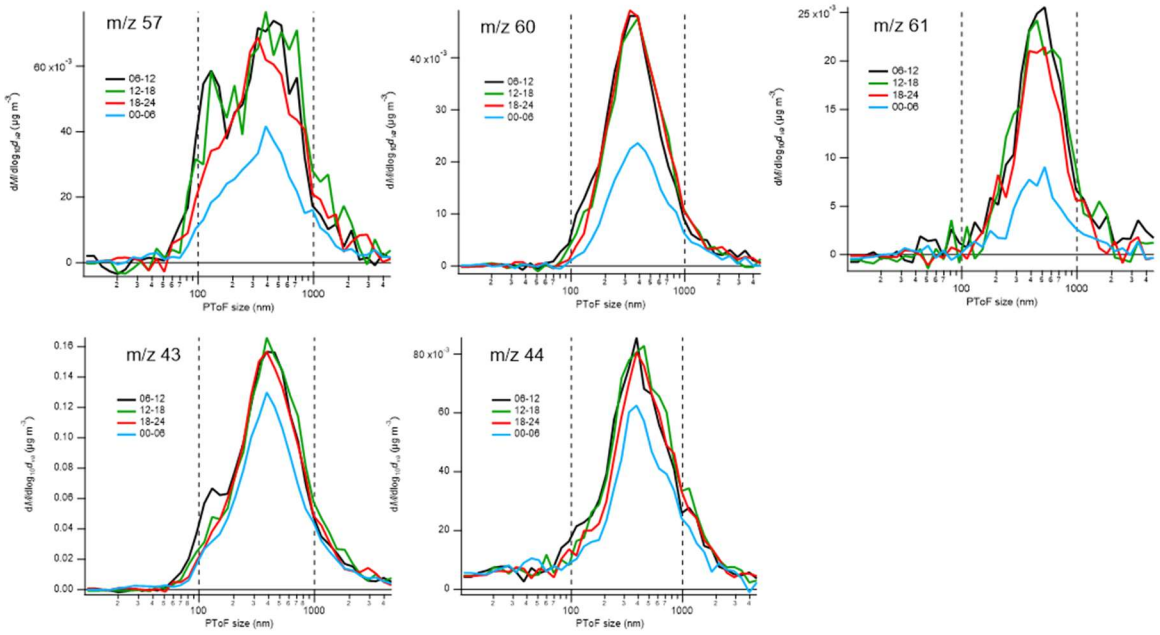

Figure S15: Average mass size distributions for m/z 57, 60, 61, 43 and 44 at different times of the day in Winter 2022. Only weekdays are included.

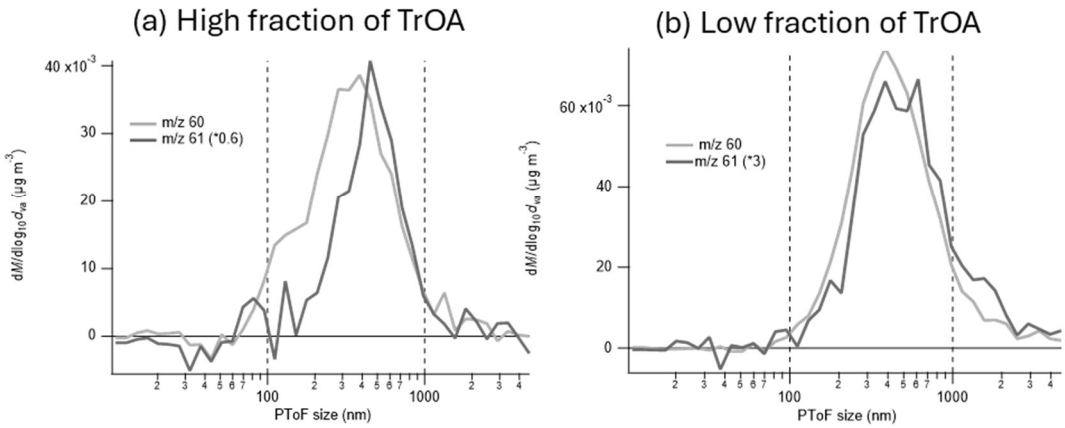

Figure S16: Average mass size distributions for m/z 60 and 61 during the periods of high (a) and low fraction (b) of TrOA in OA for Winter 2022 data.

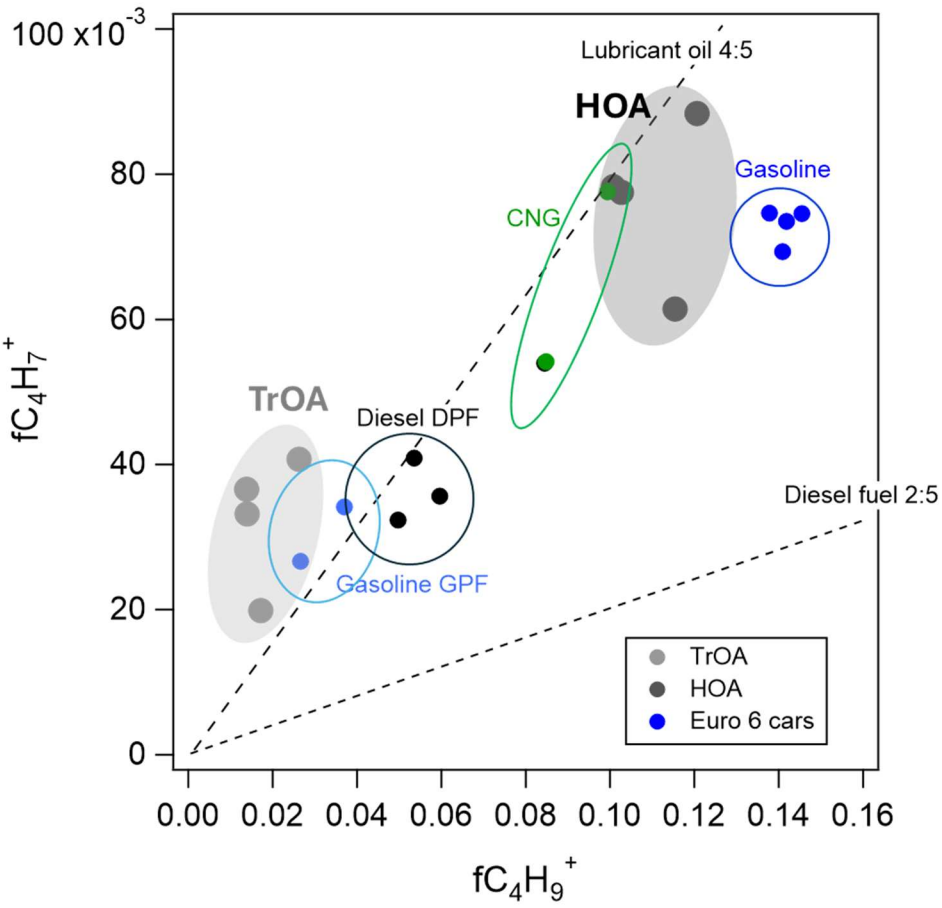

Figure S17: Scatter plots of $fC_4H_7^+$ (at m/z 55) and $fC_4H_9^+$ (at m/z 57) for TrOA and HOA in four campaigns. Additionally, $fC_4H_7^+$ and $fC_4H_9^+$ are shown for the OA from Gasoline car (without GPF), CNG car, Gasoline car with GPF, Diesel car with DPF and CNG car measured in laboratory conditions. All cars are Euro 6 level passenger cars. See details of the car measurements in Saarikoski et al. (2024). Dashed lines present the ratio for lubricant oil and diesel fuel (Canagaratna et al., 2004). GPF = gasoline particulate filter, DPF = diesel particulate filter, CNG = compressed natural gas.

References

Canagaratna, M. R., Jayne, J. T., Ghertner, D. A., Herndon, S., Shi, Q., Jimenez, J. L., Silva, P. J., Williams, P., Lanni, T., Drewnick, F., Demerjian, K. L., Kolb, C. E., and Worsnop, D. R.: Chase Studies of Particulate Emissions from in-use New York City Vehicles, Aerosol Sci. Technol., 38, 555–573, https://doi.org/10.1080/02786820490465504, 2004.

Paatero, P., and Tapper, U.: Positive matrix factorization – a nonnegative factor model with optimal utilization of error-estimates of data values, Environmetrics, 5, 111–126, https://doi.org/10.1002/env.3170050203, 1994.

Saarikoski, S., Hellén, H., Praplan, A. P., Schallhart, S., Clusius, P., Niemi, J. V., Kousa, A., Tykkä, T., Kouznetsov, R., Aurela, M., Salo, L., Rönkkö, T., Barreira, L. M. F., Pirjola, L., and Timonen, H.: Characterization of volatile organic compounds and submicron organic aerosol in a traffic environment, Atmos. Chem. Phys., 23, 2963–2982, https://doi.org/10.5194/acp-23-2963-2023, 2023.

Saarikoski, S., Järvinen, A., Markkula, L., Aurela, M., Kuittinen, N., Hoivala, J., Barreira, L. M. F., Aakko-Saksa, P., Lepistö, T., Marjanen, P., Timonen, H., Hakkarainen, H., Jalava, P., and Rönkkö, T.: Towards zero pollution vehicles by advanced fuels and exhaust aftertreatment technologies, Environ. Pollut., 347, https://doi.org/10.1016/j.envpol.2024.123665, 2024.

Teinilä, K., Saarikoski, S., Lintusaari, H., Lepistö, T., Marjanen, P., Aurela, M., Hellén, H., Tykkä, T., Lampimäki, M., Lampilahti, J., Barreira, L., Mäkelä, T., Kangas, L., Hatakka, J., Harni, S., Kuula, J., V. Niemi, J., Portin, H., Yli-Ojanperä, J., Niemelä, V., Jäppi, M., Lehtipalo, K., Vanhanen, J., Pirjola, L., Manninen, H. E., Petäjä, T., Rönkkö, T., and Timonen, H.: Measurement report: Wintertime aerosol characterization at an urban traffic site in Helsinki, Finland, Atmos. Chem. Phys., 25, 4907–4928, https://doi.org/10.5194/acp-25-4907-2025, 2025.

Ulbrich, I. M., Canagaratna, M. R., Zhang, Q., Worsnop, D. R., and Jimenez, J. L.: Interpretation of organic components from Positive Matrix Factorization of aerosol mass spectrometric data, Atmos. Chem. Phys., 9, 2891–2918, https://doi.org/10.5194/acp-9-2891-2009, 2009.